Novel ^{18}F-Labeled κ-Opioid Receptor Antagonist as PET Radiotracer: Synthesis and In Vivo Evaluation of ^{18}F-LY2459989 in Nonhuman Primates

Songye Li[1], Zhengxin Cai[1], Ming-Qiang Zheng[1], Daniel Holden[1], Mika Naganawa[1], Shu-Fei Lin[1], Jim Ropchan[1], David Labaree[1], Michael Kapinos[1], Teresa Lara-Jaime[1], Antonio Navarro[2], and Yiyun Huang[1]

[1]*PET Center, Yale University School of Medicine, New Haven, Connecticut; and* [2]*Eli Lilly and Company, Indianapolis, Indiana*

The κ-opioid receptor (KOR) has been implicated in depression, addictions, and other central nervous system disorders and, thus, is an important target for drug development. We previously developed several ^{11}C-labeled PET radiotracers for KOR imaging in humans. Here we report the synthesis and evaluation of ^{18}F-LY2459989 as the first ^{18}F-labeled KOR antagonist radiotracer in nonhuman primates and its comparison with ^{11}C-LY2459989. **Methods:** The novel radioligand ^{18}F-LY2459989 was synthesized by ^{18}F displacement of a nitro group or an iodonium ylide. PET scans in rhesus monkeys were obtained on a small-animal scanner to assess the pharmacokinetic and in vivo binding properties of the ligand. Metabolite-corrected arterial activity curves were measured and used as input functions in the analysis of brain time–activity curves and the calculation of binding parameters. **Results:** With the iodonium ylide precursor, ^{18}F-LY2459989 was prepared at high radiochemical yield (36% ± 7% [mean ± SD]), radiochemical purity (>99%), and mean molar activity (1,175 GBq/μmol; $n = 6$). In monkeys, ^{18}F-LY2459989 was metabolized at a moderate rate, with a parent fraction of approximately 35% at 30 min after injection. Fast and reversible kinetics were observed, with a regional peak uptake time of less than 20 min. Pretreatment with the selective KOR antagonist LY2456302 (0.1 mg/kg) decreased the activity level in regions with high levels of binding to that in the cerebellum, thus demonstrating the binding specificity and selectivity of ^{18}F-LY2459989 in vivo. Regional time–activity curves were well fitted by the multilinear analysis 1 kinetic model to derive reliable estimates of regional distribution volumes. With the cerebellum as the reference region, regional binding potentials were calculated and ranked as follows: cingulate cortex > insula > caudate/putamen > frontal cortex > temporal cortex > thalamus, consistent with the reported KOR distribution in the monkey brain. **Conclusion:** The evaluation of ^{18}F-LY2459989 in nonhuman primates demonstrated many attractive imaging properties: fast tissue kinetics, specific and selective binding to the KOR, and high specific binding signals. A side-by-side comparison of ^{18}F-LY2459989 and ^{11}C-LY2459989 indicated similar kinetic and binding profiles for the 2 radiotracers. Taken together, the results indicated that ^{18}F-LY2459989 appears to be an excellent PET radiotracer for the imaging and quantification of the KOR in vivo.

Key Words: ^{18}F-LY2459989; κ-opioid receptor; antagonist; PET; nonhuman primates

J Nucl Med 2018; 59:140–146
DOI: 10.2967/jnumed.117.195586

The κ-opioid receptor (KOR) is a subtype of opioid receptors (*1*), which are important drug targets in modern medicine (*2*). Early studies of the KOR focused mainly on its role in analgesia, as KOR agonists have been shown to induce significant analgesic effects without the side effects caused by μ-opioid receptor ligands (such as morphine and its analogs), especially drug dependence and, thus, the potential for abuse (*3*). However, KOR agonists have other dose-limiting side effects, such as hallucination, sedation, and dysphoria (*4,5*). More recent research found that the KOR is involved in the regulation of mood and reward systems (*6,7*), suggesting the potential use of KOR antagonists as effective therapeutics for the treatment of substance abuse, depression, and anxiety (*8,9*). A few KOR antagonists, including JDTic (*10*) and LY2456302 (currently named CERC-501), have entered clinical trials as antidepressants (Fig. 1) (*11*). Furthermore, there is evidence of KOR involvement in cognitive function and cancers (*12–15*). Hence, the development of in vivo imaging agents will help in the investigation and understanding of the KOR in diseases and the evaluation of KOR-targeted drug candidates.

PET is a powerful, noninvasive imaging technique for the investigation of physiologic and biochemical processes in the living body (*16*). In the past several years, we developed several KOR agonists and antagonists (Fig. 1) as suitable PET radiotracers (*17–20*) and tested them in nonhuman primates and in humans (*21–23*).

In binding assays in vitro, LY2459989, a fluorine-containing analog of LY2795050 with the same core structure as LY2456302, displayed a 4-fold-higher affinity (K_i, 0.18 nM) than LY2795050 and improved selectivity for the KOR over the μ-opioid receptor and the δ-opioid receptor (*20*). In PET imaging experiments in vivo, ^{11}C-LY2459989 was found to have specific binding signals more than 2-fold higher than those of ^{11}C-LY2795050 in the monkey brain. Furthermore, the replacement of chlorine in LY2795050 with fluorine in LY2459989 leads to the possibility of ^{18}F radiolabeling. We first attempted ^{18}F radiolabeling of LY2459989 using the corresponding nitro precursor (Fig. 2) and later adapted iodonium ylide chemistry (*24*) for the successful radiosynthesis of ^{18}F-LY2459989 at high radiochemical yield

Received May 12, 2017; revision accepted Jun. 28, 2017.
For correspondence or reprints contact: Songye Li, PET Center, Yale University School of Medicine, 801 Howard Ave., P.O. Box 208048, New Haven, CT 06520.
E-mail: songye.li@yale.edu
Published online Jul. 26, 2017.

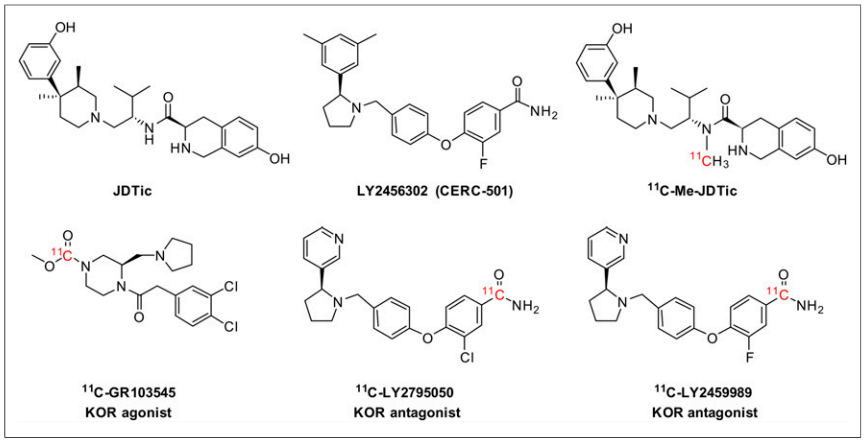

FIGURE 1. Chemical structures of KOR antagonists in clinical trials and radioligands for PET.

and molar activity (*25*). In this article, we report the in vivo evaluation of this first ^{18}F-labeled KOR antagonist PET radiotracer in nonhuman primates and its comparison with ^{11}C-LY2459989.

MATERIALS AND METHODS

Radiochemistry

The synthesis of the nitro and iodonium ylide precursors, the synthesis of the reference standard LY2458889, and detailed procedures for the radiosynthesis of ^{18}F-LY2459989 were reported previously (*25*). The final product was formulated in 1 mL of ethanol, 10 mL of saline, and 40 μL of 4.2% sodium bicarbonate solution, and the solution was filtered through a 0.22-μm membrane filter for terminal sterilization.

PET Imaging Experiments in Rhesus Monkeys

PET Scan Procedures. PET imaging experiments were performed in rhesus monkeys (*Macaca mulatta*) according to a protocol approved by the Yale University Institutional Animal Care and Use Committee. Three monkeys were used in a total of 5 scans with ^{18}F-LY2459989, including 4 baseline scans and 1 blocking scan with the KOR antagonist LY2456302 at a dose of 0.1 mg/kg. ^{18}F-LY2459989 prepared from the nitro precursor was used in 2 baseline scans, and ^{18}F-LY2459989 made from the iodonium ylide precursor was used in 3 scans, including the blocking scan. Two scans with ^{11}C-LY2459989 were also conducted in 2 of the 3 monkeys for comparison with ^{18}F-LY2459989.

In preparation for each scan, the monkey fasted overnight and was immobilized with ketamine (10 mg/kg, intramuscularly) at least 2 h before the PET scan. A venous line was inserted for administration of the radiotracer and the blocking drug on 1 limb. A catheter was placed in the femoral artery on the other limb for blood sampling. Endotracheal intubation was performed to allow the administration of isoflurane (1.5%–2.5% in oxygen). A water-jacket heating pad was used to maintain body temperature. The animal was attached to a physiologic monitor, and vital signs (heart rate, blood pressure, respirations, Spo_2, electrocardiogram, end-tidal CO_2, and body temperature) were continuously monitored.

Dynamic PET scans were performed on a Focus 220 scanner (Siemens Medical Solutions). Before radiotracer injection, a 9-min transmission scan was obtained for attenuation correction. The radiotracer was administered by an infusion pump over 3 min. Emission data were collected in list mode for 120 min and reformatted into 33 successive frames of increasing durations (6 × 10 s, 3 × 1 min, 2 × 2 min, and 22 × 5 min).

Plasma Metabolite Analysis and Input Function Measurement. Arterial blood samples were collected at preselected time points and assayed for radioactivity in the whole blood and plasma with cross-calibrated well-type γ-counters (Wizard 1480/2480; Perkin–Elmer). Six samples drawn at 5, 15, 30, 60, and 90 min were processed and analyzed to measure the radioligand metabolite profile by high-performance liquid chromatography (HPLC) using the column-switching method (*26*). Whole-blood samples in ethylenediaminetetraacetic acid tubes were centrifuged at 2,930*g* and 4°C for 5 min to separate the plasma. Supernatant plasma was collected, and the activity in 0.2-mL aliquots was counted with a γ-counter. Plasma samples were then mixed with urea (8 M) to denature plasma proteins, filtered through a 1.0-μm Whatman 13-mm CD/X syringe filter, and loaded onto an automatic column-switching HPLC system. The system contained a capture column (4.6 × 19 mm) self-packed with Phenomenex Strata-X polymeric solid-phase extraction sorbent. Elution was done with 1% acetonitrile in water at 2 mL/min for 4 min. The trapped activity in the capture column was then back flushed and eluted through a Phenomenex Luna C18(2) column (4.6 × 250 mm; 5 μm) with 40% acetonitrile in 0.1 M ammonium formate (pH 6.4; v/v) at a flow rate of 1.65 mL/min. The eluent fractions were collected with an automated fraction collector (Spectrum Chromatography CF-1). Activity in the whole blood, plasma, filtered plasma–urea mixture, filter, and HPLC eluent fractions was counted with automatic γ-counters. The sample recovery rate, extraction efficiency, and HPLC fraction recovery were monitored. The nonmetabolized parent fraction was determined as the ratio of the sum of radioactivity in fractions containing the parent compound to the total amount of radioactivity collected and fitted with an inverted γ-function and corrected for filtration efficiency. The arterial plasma input function was then calculated as the product of the total counts in the plasma and the interpolated parent fraction at each time point.

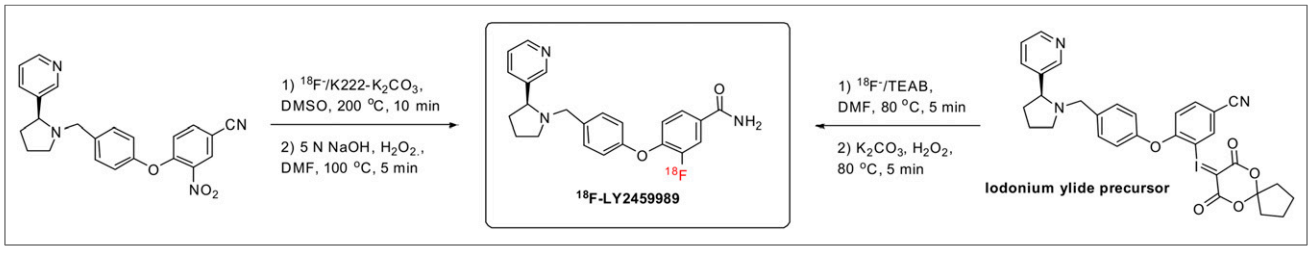

FIGURE 2. Radiosynthesis of ^{18}F-LY2459989. DMF = *N,N*-dimethylformamide; DMSO = dimethyl sulfoxide; K222 = Kryptofix 222; TEAB = tetraethylammonium bicarbonate.

Measurement of Radiotracer Free Fraction in Plasma. An ultrafiltration method was used for measuring the unbound portion (free fraction) of ^{18}F-LY2459989 in plasma. Radioactivity (~1.85 MBq) in approximately 0.1 mL of solution was mixed with 3.5 mL of an arterial blood sample taken immediately before radiotracer injection. After 10 min of incubation at room temperature, the sample was centrifuged at 2,930*g* for 5 min to partition the plasma from blood cells. The plasma sample was then loaded onto the reservoir of an ultrafiltration cartridge (Millipore Centrifree) and centrifuged at 1,228*g* for 20 min. The filtrate was collected and weighed, and counts were determined. The free fraction in plasma was determined as the ratio of the radioactivity concentration in the filtrate to the total activity in the plasma. Measurements of the free fraction in plasma were performed in triplicate for each scan.

Measurement of Lipophilicity. Lipophilicity (log *P*) was determined by a method modified from previously described procedures (*27*). Log *P* was calculated as the ratio of decay-corrected radioactivity concentrations in 1-octanol and in phosphate-buffered saline (pH 7.4; Dulbecco). Six consecutive equilibration procedures were performed until a constant value of log *P* was obtained.

Imaging Analysis and Kinetic Modeling. A representative high-resolution MR image was acquired with a Siemens 3-T Trio scanner to assist with image coregistration and anatomic localization of regions of interest (ROIs).

PET emission data were attenuation-corrected using the transmission scan, and dynamic images (33 frames over 120 min) were reconstructed using a filtered backprojection algorithm with a Shepp–Logan filter (*28*). Summed PET images were registered to MR images, and the following ROIs were defined: amygdala, brain stem, caudate, cerebellum, cingulate cortex, frontal cortex, globus pallidus, hippocampus, insula, nucleus accumbens, occipital cortex, pons, putamen, substantia nigra, temporal cortex, and thalamus. For each PET scan, radiotracer concentrations over time were measured and regional time–activity curves were generated for the ROIs.

Regional time–activity curves were fitted and analyzed with 1-tissue compartment (1TC) and 2-tissue compartment (2TC) models (*29*) as well as the multilinear analysis 1 (MA1) method (*30*). The regional distribution volume (V_T; mL·cm^{-3}) was calculated from a kinetic analysis of regional time–activity curves using the metabolite-corrected arterial plasma concentration as the input function (*31*). In the 1TC model, kinetic parameters K_1 (mL·min^{-1}·cm^{-3}) and k_2 (min^{-1}) are the rate constants of ligand transfer into and out of the brain, respectively, and the V_T values were calculated as K_1/k_2. In the 2TC model, parameters K_1 and k_2 are the constants governing the transfer of the ligand into and out of the nondisplaceable compartment, parameters k_3 (min^{-1}) and k_4 (min^{-1}) describe the respective rates of association with and dissociation from the receptors, and the V_T values were derived as $(K_1/k_2)(1 + k_3/k_4)$. The MA1 method, which is considered to be a more stable analysis method, uses only part of the data ($T > t^*$), and the selection of starting point t^* is from 10 to 60 min (10-min interval). The V_T values were calculated from the ratio of the 2 regression coefficients, $-\beta/\beta_2$. The Akaike information criterion (AIC) (*32*) and the Logan plot (*33*) were used to evaluate the goodness of fit using the MA1 method and the 1TC and 2TC models.

The nondisplaceable binding potential (BP_{ND}), a measure of the specific binding signal, was calculated from regional V_T values using the cerebellum as the reference region, that is, $BP_{ND} = (V_T \text{ of ROI} - V_T \text{ of cerebellum})/V_T$ of cerebellum. Additionally, the simplified reference tissue model (SRTM) was also tested for calculating the BP_{ND} to evaluate the possible generation of binding parameters without arterial blood samples (*34*).

The KOR occupancy by the blocking drug was obtained from an occupancy plot using the regional V_T from the baseline scan and the difference in V_T values between the baseline scan and the blocking scan according to the method of Cunningham et al. (*35*), in which the nondisplaceable volume of distribution and occupancy were assumed to be the same for all regions.

RESULTS

Radiochemistry

With the iodonium ylide precursor, ^{18}F-LY2459989 was prepared at 36% ± 7% radiochemical yield (non–decay-corrected), greater than 99% radiochemical purity, and mean molar activity of 1,175 GBq/μmol at the end of synthesis (n = 6). Total synthesis time, including purification and formulation, was 88 min.

With the nitro precursor, the average radiochemical yield of ^{18}F-LY2459989 was less than 1%, and the mean molar activity at the end of synthesis was 62 GBq/μmol (n = 3).

PET Imaging Experiments in Rhesus Monkeys

Injection Parameters. A total of 5 PET scans were performed in 3 monkeys. The injected activity was 157.4 ± 51.8 MBq, with an injected mass of 0.43 ± 0.74 μg.

Plasma Analysis. The results of the plasma analysis are shown in Figure 3. The rate of metabolism of ^{18}F-LY2459989 was moderate, with an intact parent tracer fraction of 35% ± 13% at 30 min after radiotracer injection; this value further decreased to 20% ± 7% and 13% ± 4%, respectively, at 60 and 90 min (n = 5) (Fig. 3A). After a bolus injection of ^{18}F-LY2459989, the parent radioactivity level in plasma displayed a quick increase to peak, a sharp decline phase, and then a slow decrease from 10 min onward (Fig. 3B). On the reverse-phase HPLC chromatograms, the 2 metabolites of ^{18}F-LY2459989 appeared to be more polar, with shorter retention times than the parent (Fig. 3C). The measured log *P* value of ^{18}F-LY2459989 was 3.44 (n = 1), similar to that measured for ^{11}C-LY2459989 (3.04 ± 0.37; n = 10). The free fraction of the radioligand in plasma was 4.2% ± 0.2% (n = 5), also similar to that measured for ^{11}C-LY2459989 (4.5% ± 0.6%; n = 21) (*20*).

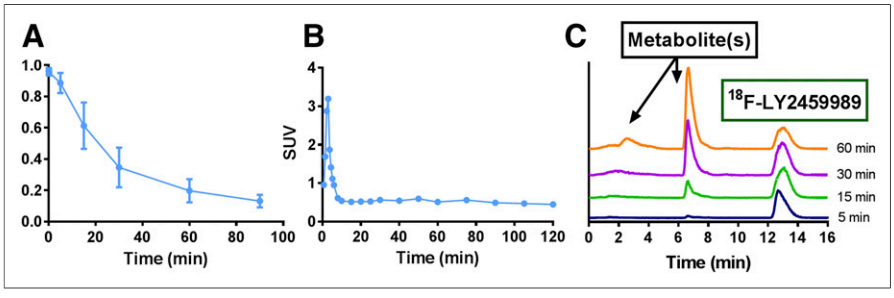

FIGURE 3. (A) Parent fraction of ^{18}F-LY2459989 in plasma. (B) Metabolite-corrected plasma activity over time. (C) HPLC chromatograms from metabolite analysis.

Brain Analysis. The PET images and regional time–activity curves of ^{18}F-LY2459989 from both baseline and blocking scans of rhesus monkeys are shown in Figure 4. In the monkey brain, ^{18}F-LY2459989 exhibited good uptake and a heterogeneous distribution in different regions (Fig. 4A, middle). The highest concentrations of the radiotracer were observed in the globus pallidus

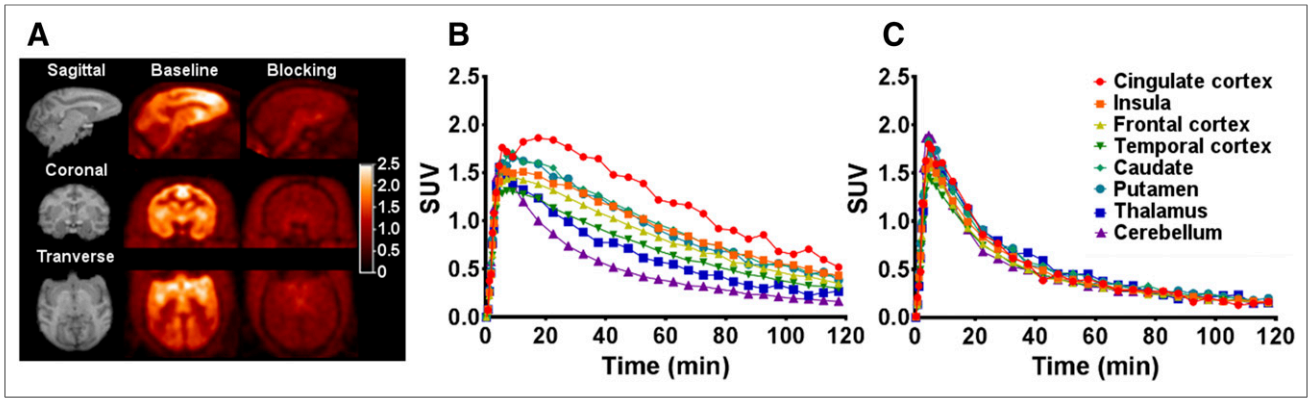

FIGURE 4. (A) MR images (left) and PET SUV images summed from 20 to 40 min after ^{18}F-LY2459989 injection for baseline scan (middle) and corresponding blocking scan with LY2456302 (0.1 mg/kg) (right). (B) Brain regional time–activity curves from baseline scan of ^{18}F-LY2459989. (C) Time–activity curves for ^{18}F-LY2459989 from blocking scan with LY2456302 (0.1 mg/kg).

and cingulate cortex, whereas the lowest uptake was seen in the cerebellum. Blocking with the KOR-specific antagonist LY2456302 at a dose of 0.1 mg/kg reduced the brain uptake to an almost homogeneous pattern across all regions (Fig. 4A, right). From the PET images, it appeared that the activity level in the skull was low and similar to that of the background, indicating no deposition of ^{18}F-fluoride in bone structures and, thus, the lack of defluorination for the radiotracer in monkeys.

The tissue kinetics of ^{18}F-LY2459989 were rapid. Regional concentrations of the radiotracer reached a peak within 20 min after injection and were followed by a moderate rate of clearance over time (Fig. 4B). After entering the monkey brain, the radiotracer localized to KOR-rich regions, such as the cortex and striatum (Fig. 4B). Pretreatment of the animal with LY2456302 at 0.1 mg/kg brought the uptake level in regions with high levels of binding to that in the region of the cerebellum with the lowest level of binding, demonstrating the blockade of ^{18}F-LY2459989–specific binding in the monkey brain (Fig. 4C).

Regional time–activity curves were processed with the 1TC and 2TC models and the MA1 method to generate the binding parameters using the metabolite-corrected plasma activity as an input function. The 2TC model showed apparently better fits to the data than the 1TC model (AIC [2TC] < AIC [1TC]); therefore, the 2TC model was considered to be a more suitable model for analyzing the imaging data. V_T values estimated with the MA1 method correlated well with those obtained from the 2TC model ($V_{T(MA1)}$ = $0.98V_{T\ (2TC)}$ + 0.16). Listed in Table 1 are regional V_T values derived from the MA1 analysis (t^*, 30 min).

Regional BP_{ND} values were calculated from MA1 V_T values using the cerebellum as the reference region and are shown in Table 2, along with those calculated from the SRTM, which showed an excellent correlation with MA1 BP_{ND} values ($BP_{ND\ (SRTM)}$ = 0.97 $BP_{ND\ (MA1)}$ + 0.03). The rank order of BP_{ND} values in various regions was as follows: globus pallidus > cingulate cortex > insula > caudate > putamen > frontal cortex > temporal cortex > thalamus > cerebellum, consistent with the reported KOR distribution in the monkey brain (*36,37*).

In the blocking study, pretreatment with LY2456302 at a dose of 0.1 mg/kg before radiotracer injection significantly reduced regional BP_{ND} values to negligible levels across the monkey brain (Table 2). Receptor occupancy calculated from the occupancy plot was 93%, and the nondisplaceable distribution volume was 3.06 mL·cm^{-3}.

Comparison of ^{18}F-LY2459989 and ^{11}C-LY2459989. Two pairs of PET scans with both ^{18}F-LY2459989 and ^{11}C-LY2459989 were obtained for the same monkeys to compare the kinetic behaviors of these 2 radiotracers. Representative PET images and regional time–activity curves (Fig. 5) demonstrated similar regional distributions and kinetics. The binding parameters for these 2 radiotracers were also very similar (Table 3).

DISCUSSION

We previously reported ^{11}C-LY2459989 as an improved KOR antagonist radiotracer with high specific binding signals in nonhuman primates (*20*). Recently, we published the results of a

TABLE 1
MA1-Derived Regional V_T Values for ^{18}F-LY2459989 in Monkey Brain

	V_T (mL·cm^{-3}) in brain region:								
Study	Globus pallidus	Cingulate cortex	Insula	Caudate	Putamen	Frontal cortex	Temporal cortex	Thalamus	Cerebellum
Baseline (n = 4)	13.61 ± 2.63	11.66 ± 2.94	9.85 ± 2.10	9.43 ± 2.27	9.05 ± 1.78	7.80 ± 1.88	7.05 ± 1.39	6.76 ± 1.18	4.62 ± 0.94
Blocking (n = 1)	4.12	3.39	3.30	3.58	3.62	3.11	3.05	3.56	3.16

Data are reported as mean or as mean ± SD.

TABLE 2
MA1- and SRTM-Derived Regional BP_{ND} Values for ^{18}F-LY2459989 in Monkey Brain

Method or model	Study	BP_{ND} in brain region: Globus pallidus	Cingulate cortex	Insula	Caudate	Putamen	Frontal cortex	Temporal cortex	Thalamus
MA1	Baseline (n = 4)	1.96 ± 0.49	1.56 ± 0.17	1.14 ± 0.19	1.08 ± 0.10	0.96 ± 0.05	0.71 ± 0.02	0.53 ± 0.07	0.47 ± 0.17
	Blocking (n = 1)	0.30	0.07	0.04	0.13	0.15	−0.01	−0.04	0.14
SRTM	Baseline (n = 4)	1.93 ± 0.33	1.51 ± 0.17	1.13 ± 0.14	1.03 ± 0.12	0.97 ± 0.05	0.68 ± 0.08	0.54 ± 0.06	0.49 ± 0.16
	Blocking (n = 1)	0.31	0.08	0.05	0.14	0.15	−0.01	−0.03	0.15

Data are reported as mean or as mean ± SD.

detailed study to optimize conditions for the radiosynthesis of ^{18}F-LY2459989, which is not readily accessible via conventional radiochemical approaches (*25*). In this article, we describe the comprehensive in vivo evaluation of this first ^{18}F-labeled KOR antagonist PET radiotracer in rhesus monkeys and its comparison with ^{11}C-LY2459989.

The novel radiotracer ^{18}F-LY2459989 was synthesized by nucleophilic radiofluorination of the nitro precursor with ^{18}F-fluoride and Kryptofix 222 (Sigma–Aldrich)–K_2CO_3 in *N,N*-dimethyl sulfoxide at 200°C and the iodonium ylide precursor with ^{18}F-fluoride and tetraethylammonium bicarbonate in *N,N*-dimethylformamide at 80°C. The radiosynthesis can be performed either manually or in a microfluidic reactor (NanoTek). On average, synthesis with the iodonium ylide precursor provides the final product, ^{18}F-LY2459989, at high radiochemical yield and purity, as well as molar activity at the end of synthesis that is much higher than that of ^{11}C-LY2459989 (means of 26 GBq/μmol for ^{11}C-LY2459989 vs. 1,175 GBq/μmol for ^{18}F-LY2459989).

In rhesus monkeys, ^{18}F-LY2459989 was metabolized at a moderate rate, with a parent fraction of 35% ± 13% at 30 min after injection (Fig. 3A). Two major radioactive metabolites that were detected in the blood appeared to be much more polar than the parent radiotracer (Fig. 3C) and, thus, were unlikely to enter the brain and complicate the quantitative analysis of PET imaging data.

^{18}F-LY2459989 had a measured log *P* of 3.44, which value fits in the range for PET radioligands that are predicted to have good permeability through the blood–brain barrier (*38*). Indeed, ^{18}F-LY2459989 readily entered the monkey brain and accumulated in regions known to have high KOR densities, such as the cortex and striatum (Figs. 4A and 4B). Regional time–activity curves demonstrated fast and reversible brain uptake kinetics. The highest tissue uptake levels were found in the globus pallidus and cingulate cortex, with SUVs of between 1.8 and 4.5, depending on the animals. Peak uptake was reached within 20 min after injection in all brain regions, indicating fast tissue kinetics for the radiotracer. In the blocking study, pretreatment of the monkey with the KOR-specific antagonist LY2456302 at a dose of 0.1 mg/kg reduced the uptake of ^{18}F-LY2459989 across all ROIs to levels similar to that in the cerebellum, thus demonstrating the binding specificity of the radiotracer in vivo.

In a comparison of kinetic models for PET data analysis, the 2TC model provided a better fit to regional time–activity curves than the 1TC model. Therefore, the 2TC model was considered to be an appropriate model for the estimation of binding parameters. A

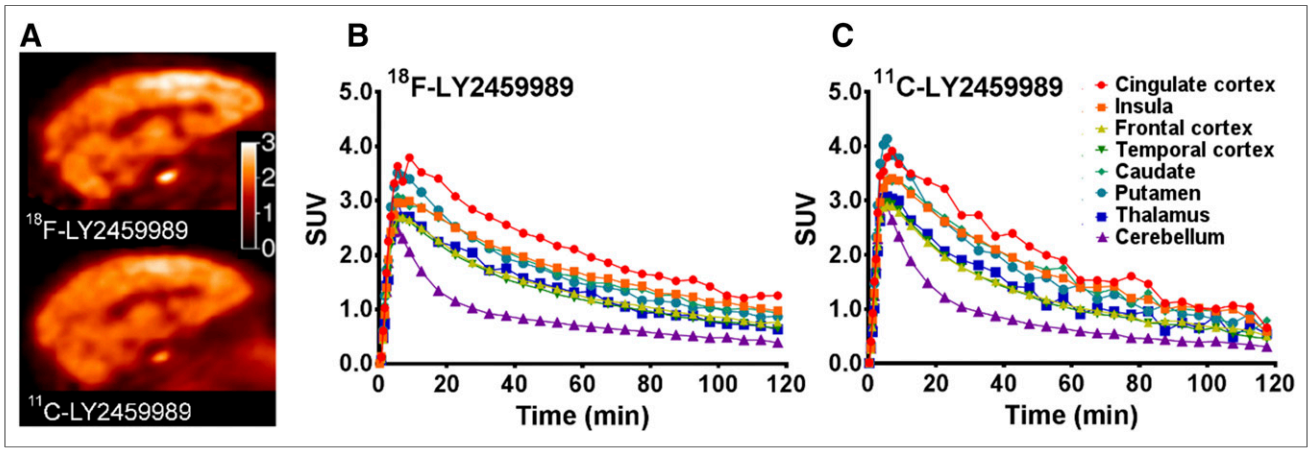

FIGURE 5. (A) PET SUV images of ^{18}F-LY2459989 (top) and ^{11}C-LY2459989 (bottom) summed from 20 to 40 min after injection. Time–activity curves of ^{18}F-LY2459989 (B) and ^{11}C-LY2459989 (C) in same monkeys.

TABLE 3
Comparison of Binding Parameters for ^{18}F-LY2459989 and ^{11}C-LY2459989 in Same Monkeys (n = 2; Baseline Scans)

Parameter	Tracer	Value in brain region: Globus pallidus	Cingulate cortex	Insula	Caudate	Putamen	Frontal cortex	Temporal cortex	Thalamus	Cerebellum
V_T (mL·cm^{-3})	^{18}F-LY2459989	14.17 ± 1.41	12.22 ± 1.94	10.11 ± 0.61	10.00 ± 1.06	9.70 ± 0.99	8.44 ± 1.29	7.50 ± 0.59	7.20 ± 0.21	4.95 ± 0.69
	^{11}C-LY2459989	11.44 ± 2.16	8.63 ± 0.06	7.57 ± 0.76	7.59 ± 0.74	7.24 ± 0.81	5.86 ± 0.06	5.50 ± 0.32	5.46 ± 0.96	3.78 ± 0.02
BP_{ND}	^{18}F-LY2459989	1.91 ± 0.69	1.46 ± 0.05	1.05 ± 0.16	1.03 ± 0.07	0.96 ± 0.07	0.70 ± 0.02	0.52 ± 0.10	0.47 ± 0.25	
	^{11}C-LY2459989	2.02 ± 0.55	1.28 ± 0.03	1.00 ± 0.19	1.01 ± 0.19	0.92 ± 0.21	0.55 ± 0.02	0.45 ± 0.08	0.44 ± 0.25	

Data are reported as mean ± SD.

further comparison of the 2TC model and the MA1 method revealed that the latter produced reliable regional V_T estimates that correlated well with those from the 2TC model, a finding that is consistent with the results of a previous kinetic modeling analysis of PET imaging data for other KOR radiotracers in nonhuman primates (*19,20*).

Previous studies with KOR radiotracers also indicated that the cerebellum can be used as a reference region to calculate the BP_{ND} in nonhuman primates. The same appeared to be true for ^{18}F-LY2459989, as regional BP_{ND} values estimated by the SRTM using the cerebellum as a reference region exhibited excellent correlations with those calculated from MA1-derived V_T values.

Given the equivalent chemical structures of ^{18}F-LY2459989 and ^{11}C-LY2459989, they behaved comparably in the same monkeys in terms of the metabolism rate (36% ± 7% vs. 30% ± 3% at 30 min after injection; n = 2), the free fraction (4.2% ± 0.2% vs. 4.0% ± 0.1%; n = 2), uptake kinetics, the regional distribution (Fig. 5), and specific binding signals, as measured by the BP_{ND} (Table 3). Both ^{18}F-LY2459989 and ^{11}C-LY2459989 provided BP_{ND} values of greater than 0.5 in most brain regions, levels of specific binding signals that can be reliably and accurately estimated by a quantitative kinetic modeling analysis. Such a characteristic is important for a suitable and effective neuroimaging radiotracer (*39*).

CONCLUSION

We successfully prepared the first ^{18}F-labeled KOR antagonist radiotracer, ^{18}F-LY2459989, and performed a detailed evaluation in nonhuman primates. This novel radiotracer exhibited favorable pharmacokinetic and in vivo binding characteristics, including an appropriate rate of metabolism, a reliably measurable free fraction in plasma, high brain uptake, fast and reversible tissue kinetics, and specific and selective binding to the KOR. A side-by-side comparison of ^{18}F-LY2459989 and ^{11}C-LY2459989 indicated similar kinetic and binding profiles for the 2 radiotracers. Overall, ^{18}F-LY2459989 afforded certain advantages over its ^{11}C-labeled counterpart, such as a longer half-life, resulting in better counting statistics at later time points of the PET scan, and more importantly, the feasibility of central production and distribution to off-site locations for use in multicenter clinical trials.

DISCLOSURE

This study was supported by grants from the National Institute of Mental Health (R21MH092664 and R33MH092664). This publication was also made possible by CTSA grant UL1 RR024139 from the National Center for Research Resources (NCRR) and the National Center for Advancing Translational Science (NCATS), components of the National Institutes of Health (NIH), and the NIH Roadmap for Medical Research. Its contents are solely the responsibility of the authors and do not necessarily represent the official view of the NIH. No other potential conflict of interest relevant to this article was reported.

ACKNOWLEDGMENT

We thank the staff at the Yale PET Center for their expert technical assistance.

REFERENCES

1. Martin WR. History and development of mixed opioid agonists, partial agonists and antagonists. *Br J Clin Pharmacol.* 1979;7(suppl 3):273S–279S.
2. Freye E, Levy JV. *Opioids in Medicine: A Systematic and Comprehensive Review on the Mode of Action and the Use of Analgesics in Different Clinical Pain States.* Dordrecht, The Netherlands: Springer; 2008.
3. Vonvoigtlander PF, Lahti RA, Ludens JH. U-50,488: a selective and structurally novel non-Mu (kappa) opioid agonist. *J Pharmacol Exp Ther.* 1983;224:7–12.
4. Pfeiffer A, Brantl V, Herz A, Emrich HM. Psychotomimesis mediated by kappa opiate receptors. *Science.* 1986;233:774–776.
5. Mucha RF, Herz A. Motivational properties of kappa and mu opioid receptor agonists studied with place and taste preference conditioning. *Psychopharmacology (Berl).* 1985;86:274–280.
6. Lutz PE, Kieffer BL. Opioid receptors: distinct roles in mood disorders. *Trends Neurosci.* 2013;36:195–206.
7. Bruijnzeel AW. Kappa-opioid receptor signaling and brain reward function. *Brain Res Rev.* 2009;62:127–146.
8. Crowley NA, Kash TL. Kappa opioid receptor signaling in the brain: circuitry and implications for treatment. *Prog Neuropsychopharmacol Biol Psychiatry.* 2015;62:51–60.
9. Carlezon WA Jr, Krystal AD. Kappa-opioid antagonists for psychiatric disorders: from bench to clinical trials. *Depress Anxiety.* 2016;33:895–906.
10. Thomas JB, Atkinson RN, Rothman RB, et al. Identification of the first *trans*-(3*R*,4*R*)-dimethyl-4-(3-hydroxyphenyl)piperidine derivative to possess highly potent and selective opioid kappa receptor antagonist activity. *J Med Chem.* 2001;44:2687–2690.
11. Mitch CH, Quimby SJ, Diaz N, et al. Discovery of aminobenzyloxyarylamides as kappa opioid receptor selective antagonists: application to preclinical development of a kappa opioid receptor antagonist receptor occupancy tracer. *J Med Chem.* 2011;54:8000–8012.
12. Loacker S, Sayyah M, Wittmann W, Herzog H, Schwarzer C. Endogenous dynorphin in epileptogenesis and epilepsy: anticonvulsant net effect via kappa opioid receptors. *Brain.* 2007;130:1017–1028.
13. Daumas S, Betourne A, Halley H, et al. Transient activation of the CA3 kappa opioid system in the dorsal hippocampus modulates complex memory processing in mice. *Neurobiol Learn Mem.* 2007;88:94–103.
14. Kharmate G, Rajput PS, Lin YC, Kumar U. Inhibition of tumor promoting signals by activation of SSTR2 and opioid receptors in human breast cancer cells. *Cancer Cell Int.* 2013;13:93.

15. Kuzumaki N, Suzuki A, Narita M, et al. Effect of kappa-opioid receptor agonist on the growth of non-small cell lung cancer (NSCLC) cells. *Br J Cancer.* 2012; 106:1148–1152.
16. Phelps ME. Positron emission tomography provides molecular imaging of biological processes. *Proc Natl Acad Sci USA.* 2000;97:9226–9233.
17. Nabulsi NB, Zheng MQ, Ropchan J, et al. [^{11}C]GR103545: novel one-pot radiosynthesis with high specific activity. *Nucl Med Biol.* 2011;38:215–221.
18. Talbot PS, Narendran R, Butelman ER, et al. ^{11}C-GR103545, a radiotracer for imaging kappa-opioid receptors in vivo with PET: synthesis and evaluation in baboons. *J Nucl Med.* 2005;46:484–494.
19. Zheng MQ, Nabulsi N, Kim SJ, et al. Synthesis and evaluation of ^{11}C-LY2795050 as a kappa-opioid receptor antagonist radiotracer for PET imaging. *J Nucl Med.* 2013;54:455–463.
20. Zheng MQ, Kim SJ, Holden D, et al. An improved antagonist radiotracer for the kappa-opioid receptor: synthesis and characterization of ^{11}C-LY2459989. *J Nucl Med.* 2014;55:1185–1191.
21. Naganawa M, Zheng MQ, Henry S, et al. Test-retest reproducibility of binding parameters in humans with ^{11}C-LY2795050, an antagonist PET radiotracer for the kappa opioid receptor. *J Nucl Med.* 2015;56:243–248.
22. Naganawa M, Zheng MQ, Nabulsi N, et al. Kinetic modeling of ^{11}C-LY2795050, a novel antagonist radiotracer for PET imaging of the kappa opioid receptor in humans. *J Cereb Blood Flow Metab.* 2014;34:1818–1825.
23. Naganawa M, Jacobsen LK, Zheng MQ, et al. Evaluation of the agonist PET radioligand [^{11}C]GR103545 to image kappa opioid receptor in humans: kinetic model selection, test-retest reproducibility and receptor occupancy by the antagonist PF-04455242. *Neuroimage.* 2014;99:69–79.
24. Rotstein BH, Stephenson NA, Vasdev N, Liang SH. Spirocyclic hypervalent iodine(III)-mediated radiofluorination of non-activated and hindered aromatics. *Nat Commun.* 2014;5:4365.
25. Cai Z, Li S, Pracitto R, et al. Fluorine-18-labeled antagonist for PET imaging of kappa opioid receptors. *ACS Chem Neurosci.* 2017;8:12–16.
26. Hilton J, Yokoi F, Dannals RF, Ravert HT, Szabo Z, Wong DF. Column-switching HPLC for the analysis of plasma in PET imaging studies. *Nucl Med Biol.* 2000;27:627–630.
27. del Rosario RB, Jung YW, Baidoo KE, Lever SZ, Wieland DM. Synthesis and in vivo evaluation of a ^{99m}/^{99}Tc-DADT-benzovesamicol: a potential marker for cholinergic neurons. *Nucl Med Biol.* 1994;21:197–203.
28. Shepp LA, Logan BF. The Fourier reconstruction of a head section. *IEEE Trans Nucl Sci.* 1974;21:21–43.
29. Gunn RN, Gunn SR, Cunningham VJ. Positron emission tomography compartmental models. *J Cereb Blood Flow Metab.* 2001;21:635–652.
30. Ichise M, Toyama H, Innis RB, Carson RE. Strategies to improve neuroreceptor parameter estimation by linear regression analysis. *J Cereb Blood Flow Metab.* 2002;22:1271–1281.
31. Innis RB, Cunningham VJ, Delforge J, et al. Consensus nomenclature for in vivo imaging of reversibly binding radioligands. *J Cereb Blood Flow Metab.* 2007;27:1533–1539.
32. Akaike H. A new look at the statistical model identification. *IEEE Transactions on Automatic Control.* 1974;19:716–723.
33. Logan J, Fowler JS, Volkow ND, Wang GJ, Ding YS, Alexoff DL. Distribution volume ratios without blood sampling from graphical analysis of PET data. *J Cereb Blood Flow Metab.* 1996;16:834–840.
34. Lammertsma AA, Hume SP. Simplified reference tissue model for PET receptor studies. *Neuroimage.* 1996;4:153–158.
35. Cunningham VJ, Rabiner EA, Slifstein M, Laruelle M, Gunn RN. Measuring drug occupancy in the absence of a reference region: the Lassen plot re-visited. *J Cereb Blood Flow Metab.* 2010;30:46–50.
36. Sim-Selley LJ, Daunais JB, Porrino LJ, Childers SR. Mu and kappa1 opioid-stimulated [^{35}S]guanylyl-5′-*O*-(gamma-thio)-triphosphate binding in cynomolgus monkey brain. *Neuroscience.* 1999;94:651–662.
37. Tomasi G, Nabulsi N, Zheng MQ, et al. Determination of in vivo B_{max} and K_d for ^{11}C-GR103545, an agonist PET tracer for kappa-opioid receptors: a study in nonhuman primates. *J Nucl Med.* 2013;54:600–608.
38. Seelig A, Gottschlich R, Devant RM. A method to determine the ability of drugs to diffuse through the blood-brain-barrier. *Proc Natl Acad Sci USA.* 1994;91:68–72.
39. Laruelle M, Slifstein M, Huang Y. Relationships between radiotracer properties and image quality in molecular imaging of the brain with positron emission tomography. *Mol Imaging Biol.* 2003;5:363–375.